Evaluation of Sol-Gel Processed $BaO \cdot nAl_2O_3$ Materials as NO_x Traps

Chaitanya K. Narula, Sabine R. Nakouzi, and Ruowen Wu
Dept. of Chemistry, Ford Motor Co., Dearborn, MI 48121

Christian T. Goralski, Jr.,
Dept. of Chemical Engineering, Ford Motor Motor Co., Dearborn, MI 48121

Lawrence F. Allard, Jr.
HTML, Oak Ridge National Laboratory, Oak Ridge, TN 37831

Among various strategies to treat NO_x, trapping is considered an economical, consumer transparent approach for gasoline engines. The conventional NO_x traps are based on alkaline-earth metal impregnated alumina. These traps work well, but cannot sustain their NO_x trapping efficiency after repeated exposure to high temperatures during regeneration. In search of thermally stable materials, a series of sol-gel processed $BaO \cdot nAl_2O_3$ ($n = 1, 4, 6$) materials including $BaO \cdot 6Al_2O_3$ molecular sieves were synthesized and evaluated as NO_x traps using simulated exhaust at a 25,000 h^{-1} space velocity. Changes in structure and surface properties occurring on thermal treatment of sol-gel processed $BaO \cdot nAl_2O_3$ materials significantly affect the NO_x trapping efficiency of these materials. Among these materials, sol-gel processed and precious metal impregnated $BaO \cdot 6Al_2O_3$ powder offers the optimum combination of thermal stability and NO_x trapping efficiency. We deposited this powder on a honeycomb substrate, impregnated it with 2% Pt and 0.4% Rh, and reevaluated it. The NO_x trapping efficiency of this catalyst is 95% (cf. 75% for the powder) at 310°C. Our data on $Pt/BaO \cdot 6Al_2O_3$ also suggest that the optimum lean cycle length for this class of NO_x traps is 1 min. The efficiency of NO_x traps decreases rapidly and falls in 10–20% range with an alternating 5 min lean cycle and 1 min rich cycle.

Introduction

Modern gasoline vehicles are equipped with three-way catalysts for the treatment of exhaust gases (Narula et al., 1996). Three-way catalysts operate efficiently in a narrow window where the ratio of oxidizing to reducing species is close to stoichiometric. The operation of these vehicles under lean conditions is thermodynamically more efficient and leads to improved fuel economy and reduced hydrocarbon (HC) and carbon monoxide (CO) emissions. The trade-off is that the concentration of NO_x ($NO + NO_2$) in the exhaust stream increases significantly, because the state-of-the-art "three-way" catalyst cannot reduce NO_x to benign gases under oxidizing conditions. Furthermore, compression ignited diesel engines, which also provide better fuel economy, operate in lean conditions and release higher amounts of NO_x than stoichiometric gasoline engines. The reduction of NO_x under oxidizing conditions is counter-intuitive and a catalyst system that can reduce NO_x from cold-start to 600°C is yet to be found. Partial catalytic reduction of NO_x for diesel engines under oxidizing conditions can be carried out in a narrow temperature range using a Pt on alumina catalyst after startup and a Cu-ZSM-5 catalyst during normal operation (Adams et al., 1996; Narula et al., 2000).

Among other strategies to treat NO_x, trapping is considered an economically viable, consumer transparent approach for gasoline engines (Katoh et al., 1994). In this strategy, NO_x is trapped during the normal lean operation of an engine. Regeneration of the trap is carried out by short pulses of engine operation in rich mode leading to release and subse-

Correspondence concerning this article should be addressed to C. K. Narula.

quent reduction of the trapped NO_x. The commercial trap materials are prepared by impregnating γ-alumina with nitrates of alkali metals and alkaline earths followed by platinum. The mechanism of trapping is believed to involve oxidation of NO_x leading to formation of alkali metal nitrates that readily decompose during the short rich cycle (Hepburn et al., 1996; Kobayashi et al., 1997; Mahzoul et al., 1999). Unfortunately, sulfur dioxide present in the exhaust is also oxidized and trapped along with NO_x. The decomposition of the trapped sulfates requires a much higher temperature leading to sintering, and a gradual but persistent reduction in the performance of the traps. Thus, there is a need for materials that can tolerate a high temperature regeneration cycle in an exhaust environment formed in the rich cycles.

We initiated this study as a continuation of our earlier work on the incorporation of alkaline earths and lanthanides by a sol-gel process employing heterometallic alkoxide precursors (Narula, 1995, 1997, 1999). After drying, these gels are amorphous and form poorly crystallized mixed-metal oxides. In this report, we describe our results on the preparation and characterization of alumina materials containing barium oxide using various sol-gel techniques. A comparison of the physical properties and lean burn NO_x trapping efficiency of sol-gel processed materials with impregnated materials is also presented.

Experimental Studies

All preparations were carried out in an inert atmosphere using a dry box and standard vacuum line techniques to prevent hydrolysis of alkoxides by atmospheric humidity. Solvents were carefully dried and distilled before use. Commercial $Al(O^iC_3H_7)_3$ was purified by distillation. Alkaline-earth-containing alkoxides were prepared by a modified literature procedure (Mehrotra et al., 1978). Tergitol 15-S-12 (alkyloxypolyethyleneoxyethanol, $C_{12\text{-}14}H_{25\text{-}29}O(CH_2CH_2O)_xH$) was used as received from Union Carbide.

Thermogravimetric analysis (TGA) was carried out on a Perkin-Elmer TA7 instrument. Infrared spectra were recorded on a Perkin-Elmer system 2000 instrument. X-ray powder diffraction patterns (XRD) of samples were recorded on a Scintag diffractometer. BET surface areas were measured on a Micrometrics ASAP 2400 instrument.

The physical properties of gels after thermal treatment at ≥ 600°C are summarized in Table 1.

Preparation of Alumina Gel (SG): Alumina gel was prepared according to a literature procedure and fired at 600°C (Leenars et al., 1984).

Preparation of Gels from $Ba[Al(O^iPr)_4]_2$: $Ba[Al(O^iC_3H_7)_4]_2$ (3.0 g) was dissolved in 2-propanol (25 mL) and the reaction mixture was cooled to -78°C. Water (eight equivalents) mixed with 2-propanol was slowly added to the reaction mixture with stirring. The stirring was stopped and the reaction mixture was slowly warmed to room temperature that resulted in the formation of a gel. The volatiles were removed and the xerogel was collected. The resulting powder was calcined to 600°C at a rate of 10°C/min. and held at that temperature for four hours. The sample contains Ba and Al in 1:2 ratio (HBA1). The other two samples containing barium and aluminum in 1:4 (HBA2) and 1:12 (HBA3) ratio were prepared by mixing an appropriate amount of $Al(O^iC_3H_7)_3$ with $Ba[Al(O^iC_3H_7)_4]_2$ prior to hydrolysis.

HBA1: The HBA1 gels show a 12.5% weight loss in the 30–250°C range in its thermogravimetric analysis (TGA). A 2% weight loss occurs in the 250–400°C range and no additional weight loss is observed in the 400–900°C range. The BET surface area of HBA1 after heating at 300°C (rate 10°C/min, hold 4 h) is 80 m^2/g and reduces to 49 m^2/g after sintering at 600°C for 4 h and to 10 m^2/g after sintering at 900°C. The corresponding average pore diameters of the powder are 98 Å and 200 Å after thermal treatment at 600 and 900°C, respectively. X-ray powder diffraction (XRD) of the powder (Figure 1), after heating at 600°C, shows diffraction peaks due to $BaCO_3$ (JCPDS No. 71-2394). After heating at 900°C, the XRD of the sample (Figure 1) shows diffraction peaks due to $BaAl_2O_4$ (JCPDS No. 17-0306).

HBA2: The TGA of HBA2 gels show a weight loss of 22% below 400°C. No additional weight loss is observed in

Table 1. Properties of $BaO \cdot n Al_2O_3$ Materials

Materials	Name	Precursors	Sintering Temp. (°C)	BET Surface Area (m^2/g)	Avg. Pore* (Å)	Crystalline Phases (from XRD)
$BaO \cdot Al_2O_3$	HBA1	$Ba[Al(O^iC_3H_7)_4]_2$	600	49	98	$BaCO_3$
			900	10	200	$BaAl_2O_4$
$BaO \cdot 2Al_2O_3$	HBA2	$Ba[Al(O^iC_3H_7)_4]_2$ +	600	133	65	$BaCO_3$
		$Al(O^iC_3H_7)_3$	900	58	115	$BaAl_2O_4$
$BaO \cdot 6Al_2O_3$	HBA3	$Ba[Al(O^iC_3H_7)_4]_2$ +	600	190	40	γ-Al_2O_3
		$Al(O^iC_3H_7)_3$	900	126	57	$BaAl_2O_4 + \gamma$-Al_2O_3
MS-$BaO \cdot 6Al_2O_3$	MSBA3	$Ba[Al(O^iC_3H_7)_4]_2$ +	600	319	54	–
		$Al(O^iC_3H_7)_3$ +	900	186	59	–
		Tergitol 15-S-12				
$BaO \cdot 6Al_2O_3 \cdot CeO_2$	HBACe	$Ba[Al(O^iC_3H_7)_4]_2$ +	600	139	43	$BaCO_3 + CeO_2 +$
		$Al(O^iC_3H_7)_3$ +				γ-Al_2O_3
		$Ce[Al(O^iC_3H_7)_4]_3$	900	83	71	$BaAl_2O_4 + \gamma$-Al_2O_3
						$+ CeO_2$
$BaO \cdot 6Al_2O_3$	IBA3	$Ba(NO_3)_2$ +	750	86	57	$BaAl_2O_4$
		γ-Al_2O_3	900	76	80	$BaAl_2O_4 + \gamma$-Al_2O_3

*BJH desorption pore diameter.

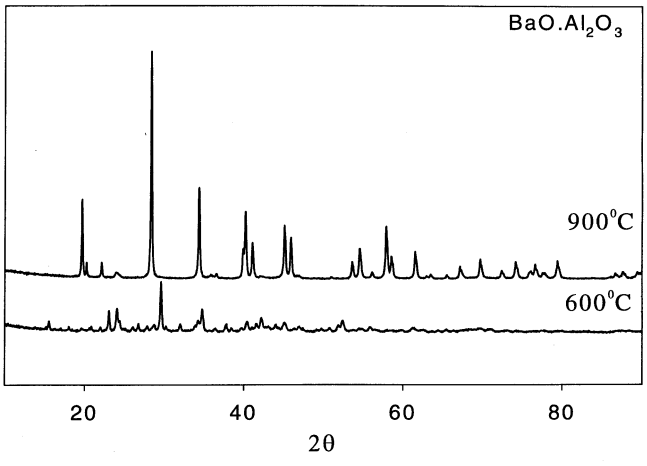

Figure 1. X-ray powder diffraction of $BaO \cdot Al_2O_3$.

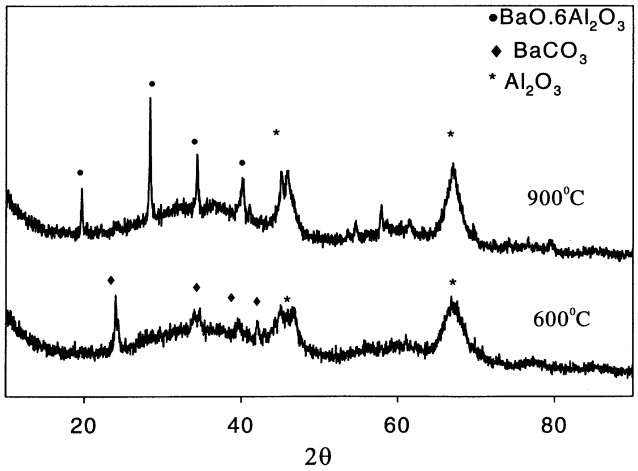

Figure 3. X-ray powder diffraction of $BaO \cdot 6Al_2O_3$.

400–900°C range. Sintering at 600°C for 4 h furnishes a powder of BET surface area of 133 m^2/g and BJH desorption pore diameter of 65 Å. The XRD of the powder (Figure 2) shows diffraction peaks due to $BaCO_3$ (JCPDS No. 71-2394). Further sintering at 900°C results in a powder of 58 m^2/g BET surface area and 115 Å BJH desorption pore diameter. The XRD of the powder (Figure 2) shows diffraction peaks due to $BaAl_2O_4$ (JCPDS No. 17-0306).

HBA3: The TGA of HBA3 gels show a weight loss of 25% below 550°C. The BET surface area of the powder after sintering at 600°C for 4 h is 190 m^2/g and the BJH desorption pore diameter is 40 Å. XRD (Figure 3) shows broad weak diffraction peaks (particle size calculated from the Scherrer formula is 33 Å) that can be assigned to γ-alumina. Further sintering at 900°C results in a powder of BET surface area of 126 m^2/g and BJH desorption pore diameter of 57 Å. The XRD of the powder still shows broad peaks assigned to γ-alumina. Additional sharp peaks due to $BaAl_2O_4$ (JCPDS No. 17-0306) can be seen suggesting that the crystallization of $BaAl_2O_4$ has begun at this temperature. These observations are different from the previous work of Arai et al. who claim that $BaO \cdot 6Al_2O_3$, prepared by a sol-gel process employing a mixture of $Ba(OR)_2$ and $Al(OR)_3$, is an amorphous powder that does not crystallize even after sintering at 1,000°C (Machida et al., 1988).

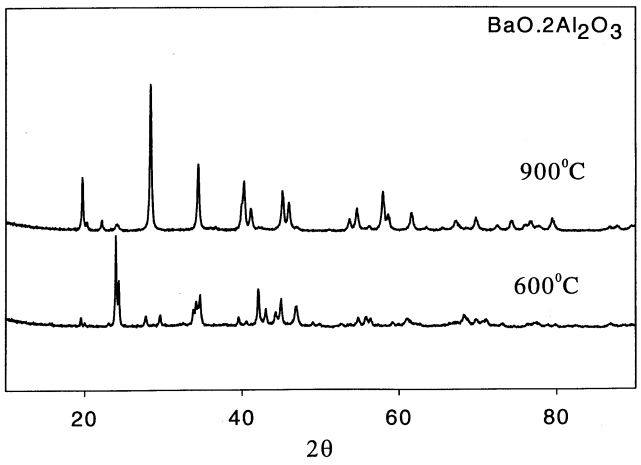

Figure 2. X-ray power diffraction of $BaO \cdot 2Al_2O_3$.

Template assisted gelation of $Ba[Al(O^iC_3H_7)_4]_2$ and $Al(O^iC_3H_7)_3$ (MSHBA3)

A solution of water (2.88 g) in 30 mL sec-butanol was added dropwise to a solution of $Ba[Al(O^iC_3H_7)_4]_2$ (2.722 g), $Al(O^iC_3H_7)_3$ (8.384 g), and Tergitol 15-S-12 (15.5 g) in sec-butanol (46 mL). The reaction mixture was diluted with sec-butanol (20 mL) and stirred for 16 h. The gel was separated by filtration, washed several times with ethanol, and air dried overnight. The resulting powder was heated to 600°C at 2°C/min and held at that temperature for 4 h.

The MSHBA3 gels show a weight loss of 25% in 30–400°C range in its TGA. The BET surface area after firing at 600°C is 319 m^2/g. The BJH desorption pore diameter is 54 Å. Mesoporosity in this material is illustrated by the N_2 adsorption/desorption isotherm and the pore-size distribution (Figure 4). The transmission electron micrograph of the sample (Figure 5) is equivalent to MSU-X alumina images reported previously for alumina (Bagshaw et al., 1995, 1996; Wenzhong and Pinnavaia, 1998). The materials are amorphous after calcining at 900°C. The molecular sieve structure starts to fail at this temperature as shown by the TEM image which starts to lose worm like motif. The BET surface area also decreases to 186 m^2/g, but the material remains amorphous.

Preparation of $BaO \cdot 6Al_2O_3 \cdot CeO_2$ (HBACe)

Ba (0.956 g) was added to a solution of $Ce[Al(O^iC_3H_7)_4]_3$ (3.956 g) and $Al(O^iC_3H_7)_3$ (14.45 g) in $^iC_3H_7OH$ (70 mL) and the reaction mixture was heated under reflux for 1.5 h. The resulting bright yellow solution was poured into H_2O (100 mL) at 80°C. The volatiles were removed by evaporation at 80°C to obtain a light yellow powder that was gradually heated to 600°C at a rate of 2°C/min and held at that temperature for 4 h.

Sintering HBACe gels at 600°C for 4 h furnishes powders of BET surface area of 139 m^2/g and BJH desorption pore

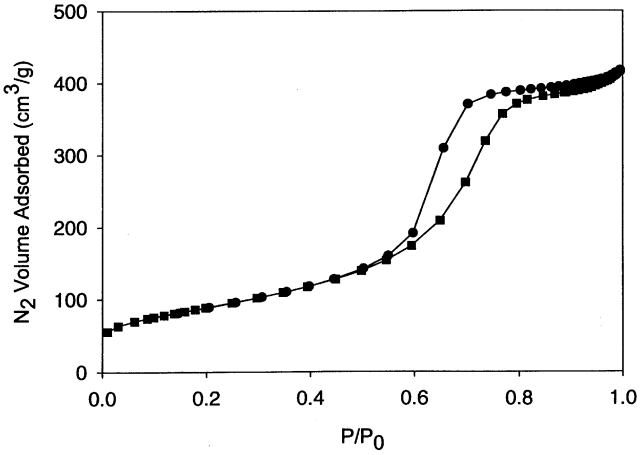

Figure 4. N_2 adsorption-desorption isotherms of $BaO \cdot 6Al_2O_3$ molecular sieves assembled in the presence of Tergitol 15-S-12.

diameter of 43 Å. The XRD of this powder (Figure 6) shows it to be poorly crystalline materials with diffraction peaks that can be assigned to $BaCO_3$ (JCPDS No. 71-2394), CeO_2 (JCPDS No. 81-0792) and a broad peak at $2\theta = 67°$ due to γ-alumina (JCPDS No. 10-425). The CeO_2 diffraction peaks are broad due to small particle size (30–37 Å, from Scherrer formula).

Preparation of 20% BaO on γ-alumina (IBA3)

$Ba(NO_3)_2$ (2.61 g) was dissolved in water (30 mL) and added to commercial γ-alumina (6.12 g). The slurry was slowly dried to a powder and the powder was calcined at a rate of 10°C/min to 750°C and held at the temperature for 4 h.

The IBA3 sample exhibits a surface area of 86 m^2/g and BJH desorption pore diameter of 57 Å after sintering at 750°C. The baria to alumina ratio in IBA3 is identical to that in HBA3. The XRD of the impregnated sample shows diffraction peaks due to barium aluminate the sintering at °C.

Platinum impregnation

A solution of chloroplatinic acid in water was added to the calcined powders of $BaO \cdot nAl_2O_3$ xerogels to deposit 1% (wt) Pt by an incipient wetness technique. The resulting slurry was dried first at room temperature and then at 105°C for 1 h. The powder was then transferred to a furnace and calcined at a rate of 2°C/min. to 500°C and held at that temperature for 4 h.

Preparation of $PtRh/BaO \cdot 6Al_2O_3 \cdot CeO_2$

A solution of rhodium nitrate in water was added to the calcined powders of $Pt/BaO \cdot nAl_2O_3 \cdot CeO_2$ materials to deposit 1% (wt) Rh by an incipient wetness technique. The resulting slurry was first dried at room temperature and then at 105°C for 1 h. The powder was then transferred to a furnace and calcined at a rate of 2°C/min. to 500°C and held at that temperature for 4 h.

Measurement of the NO_x adsorption capacity of NO_x trap materials in steady state

The overall NO_x capacity of each sample at 380°C was determined by volumetric adsorption of NO_2 using a Micrometrics ASAP 2010 chemisorption apparatus. Approximately 200 mg of each sample was placed in a quartz sample tube and evacuated for 60 min. at 400°C. The sample was then oxidized in pure oxygen at 400°C to remove any surface impurities and subsequently reduced in pure hydrogen at 400°C for 60 min. The temperature was then stabilized at 380°C and the total NO_2 capacity of each sample was measured by measuring the uptake of pure NO_2 as a function of pressure. At $T = 380$°C and $P = 0.1$ atm, the equilibrium constant for NO-NO_2 inter conversion is 0.2 This means that about 30% of NO_2 will be dissociated at equilibrium. However, the dosing

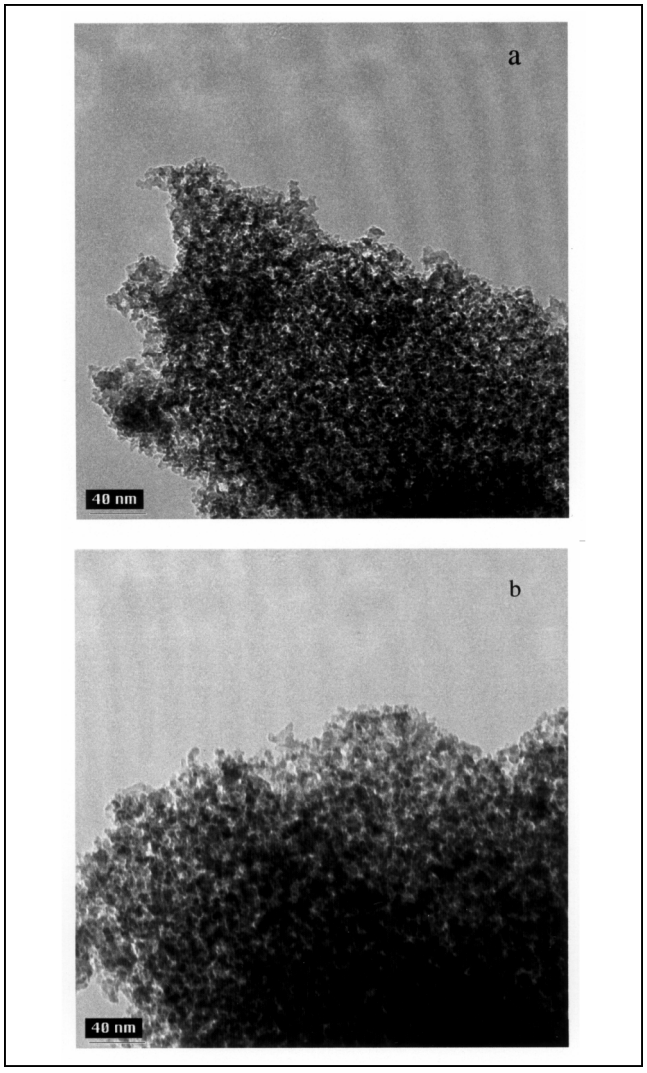

Figure 5. TEM of template assisted sol gel processed $BaO \cdot 6Al_2O_3$ after sintering at (a) 600°C and (b) 900°C.

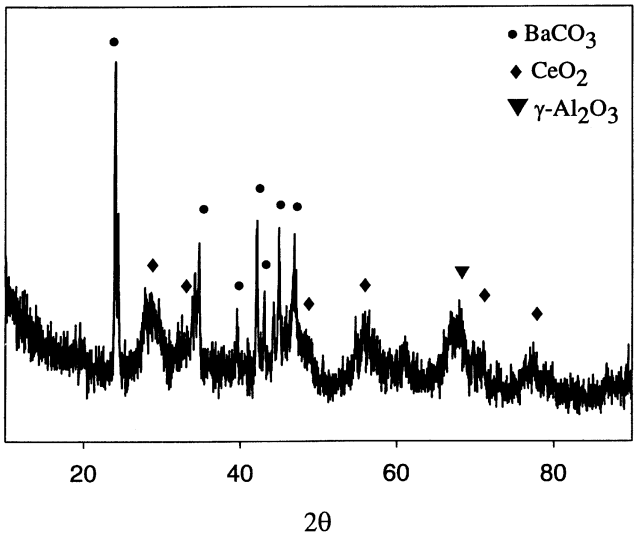

Figure 6. X-ray powder diffraction of $BaO \cdot 6Al_2O_3 \cdot CeO_2$.

time is only 60 s and the uptake of NO_2 is very fast which shifts the equilibrium towards the NO_2. A simple calculation using GRI-mech predicts less than 1 ppm NO after 60 s at 380°C starting from NO_2. Thus, the NO-NO_2 interconversion does not introduce error in the capacity measurements. The results of these experiments are summarized in Table 2.

Measurement of NO_x trapping efficiency in a dynamic flow

A brief description of test equipment and procedure is as presented in the following paragraphs.

Test Procedure: Catalytic trapping activity measurements on powders were obtained using an integral flow reactor (Hoard and Balmer, 1998). The flow reactor was charged with a powdered NO_x trap sample or the honeycomb and heated to the desired temperature (220, 310, 380, 450, or 600°C). Simulated exhaust (Table 3, gases were supplied by Michigan Airgas) was flowed through the reactor. The space velocity (25,000 h^{-1}) for the test powders is calculated by dividing gas-flow rate with the volume of the powder container while that for the honeycomb was calculated by dividing gas-flow rate with the volume of the honeycomb. The switch from lean to rich cycles is accomplished by turning off O_2 and turning on CO/H_2 (the balance is made up with N_2). The output gas mixture was diluted with nitrogen (dilution factor 15.635) and the gas concentrations were measured using an IR-based system described in the succeeding section.

Table 2. Steady State NO_x Adsorption Capacity of $BaO \cdot nAl_2O_3$ Materials

Materials	NO_2 Capacity [cm^3 (STP/g) at 760 mm Hg]	NO_2 Capacity (10^{-6} mol/g)
Pt/HBA1	4.7	486
Pt/HBA2	7	406
Pt/HBACe	10.8	312
Pt/HBA3	10.9	210
Pt/MSHBA	9.1	482

Table 3. Simulated Exhaust Composition and Test Conditions for Lean Burn NO_x Trap Materials*

Input to Reactor	Units	Condition
NO	ppm	500
CO	ppm	7,500
O_2	%	6
CO_2	%	10
SO_2	ppm	0 (off) or 9 (on)
H_2O	%	8
HC 3:1 C_3H_6:C_3H_8	ppm	120
H_2	ppm	2,500
N_2	cm^3/min	950
Target reactor flow	cm^3/min	1,330
Amount of trap powder	% (wt.)	34
Diluent powder		α-alumina
Amount of diluent	% (vol.)	66
Calc. space velocity	h^{-1}	25,000

*The CO and O_2 input is alternated with one minute hold time.

The test results on trap materials, deposited on honeycombs, are a better indicator of performance on a vehicle. However, the fabrication of honeycomb catalyst (Narula et al., 1996) of a large number of experimental materials is not practical. Instead, we selected sol-gel processed $PtRh/BaO \cdot 6Al_2O_3$ powder, based on tests on powders, for honeycomb catalyst fabrication and evaluation. The test materials were exposed to alternating lean ($R = 22.22$) and rich cycles ($R = 9.13 \times 10^{-3}$) and post-test materials gas mixture was analyzed. Here, R represents a ratio of reducing to oxidizing gases (Gandhi et al., 1976) and is calculated using the following formula: $R = \{[CO] + [H_2] + 9[C_3H_6] + 10[C_3H_8]\}/\{2[O_2] + [NO_x]\}$.

The NO_2 trapping efficiency is calculated using the following formula: $[NO_x]_{input}$-$[NO]_{output}$-$[NO_2]_{output}/[NO_x]_{input}$-$[NO]_{output}$ (Trapped NO_2/Input NO_2). There were no other nitrogen containing species (such as N_2O, HONO) in the temperature range of interest (310–380°C) and were not taken into consideration.

Analysis Equipment: In our system, either standard gas analyzers or a FTIR emissions analyzer is used for the analysis of gas mixture. We used FTIR emissions analyzer for our experiments due to its versatility and employed standard gas analyzers to get oxygen analysis (Hoard and Balmer, 1998). Here, we summarize the description of an FTIR emissions analyzer that is capable of monitoring up to 50 individual components (Gierczak et al., 1991).

The FTIR emissions analyzer contains three major components: an IR spectrometer (Nova-Cygni 120 model, Mattson Instruments), the data acquisition and processing system, and associated sampling hardware. The gases pass through a variable pathlength, multipass gas cell (Wilks, 20 Meter, Model 9020) with potassium bromide windows. The gas cell is exclusively set at the 14th order setting (21.75 m) to improve the sensitivity of the system for all chemical species. A computer equipped with an array processor controls data acquisition and data processing. The data acquisition and processing routines were developed by Butler et al. at Ford Motor Co. and licensed to Mattson Instruments Co. The system allows us to individually monitor N_2O, NO, NO_2, and HONO species in the gas mixture.

Results and Discussion

After a cold start, it takes about 120 s for the catalysts to attain the light-off temperature (Narula et al., 1996). There is sufficient concentration of hydrocarbons in the exhaust of a lean gasoline or diesel engine to reduce about 60% NO_x in the presence of Pt/alumina in a narrow temperature range of 200–250°C (Adams et al., 1996; Narula et al., 2000). Above this temperature, the oxidation of hydrocarbon and CO becomes highly efficient (Eqs. 1–3) and they are not available to participate in the NO_x reduction

$$2C_3H_6 + 9O_2 \rightarrow 6CO_2 + 6H_2O \quad (1)$$

$$C_3H_8 + 5O_2 \rightarrow 3CO_2 + 4H_2O \quad (2)$$

$$CO + O_2 \rightarrow 2CO_2 \quad (3)$$

The NO_x traps collect this NO_x in the lean cycle. The NO_x trapping mechanism (Hepburn et al., 1996; Kobayashi et al., 1997; Mahzoul et al., 1999) has been proposed to involve platinum catalyzed oxidation of NO_x to NO_2, the formation of NO_3^-, and finally the trapping as nitrates. The formation of nitrate can occur on reaction with water. Thus, this pathway will be identical to the pathway for the manufacture of nitric acid (King, 1994). Among other pathways, the NO_2 can also react with the hydrated barium or aluminum oxide surface. Since barium oxide readily reacts with CO_2 to form barium carbonate, a reaction of NO_3^- with barium carbonate will lead to the formation of nitrate and release of CO_2. All these reaction pathways are quite facile and can occur simultaneously.

The NO_x traps have limited capacity and need to be regenerated by operating engine in a rich cycle. In rich cycles, reductants in the simulated exhaust reduce all of the NO_x (Eqs. 4–6).

$$2NO + 3H_2 + 2CO \rightarrow 2CO_2 + 2NH_3 \quad (4)$$

$$2NO + 2CO \rightarrow 2CO_2 + N_2 \quad (5)$$

$$2NO + 2H_2 \rightarrow 2H_2O + N_2 \quad (6)$$

Since the thermal decomposition of NO_2 begins at 150°C and is complete at 600°C, the efficiency of NO_x trap can be expected to drop rapidly at temperatures close to 600°C. In addition to temperature, the NO_x trap efficiency depends on the availability of barium for reaction with NO_3^-. This availability of barium, in turn, can depend on the factors such as concentration of barium, structure of $BaO \cdot Al_2O_3$ materials, and oxidation facilitators such as cerium oxide. In the subsequent sections, we describe the structural variations and a comparison of trapping efficiencies of various $BaO \cdot nAl_2O_3$ powders impregnated with platinum. Among these materials, amorphous $BaO \cdot 6Al_2O_3$ powder, impregnated with precious metals, exhibited the optimum combination of thermal stability and trapping efficiency. We deposited this powder on honeycomb piece and reevaluated its trapping efficiency. We close the discussion with a comparison of our results on the sulfur dioxide poisoning of $Pt/BaO \cdot 6Al_2O_3$ and $Pt/CeO_2 \cdot BaO \cdot 6Al_2O_3$ powders.

NO_x traps

One can calculate the total amount of NO_x that can be trapped by a NO_x trap from the amount of barium in the trap washcoat. However, all of the barium is not available for reaction with NO_x. Steady-state adsorption experiments, while providing a good estimate of the NO_x trap capacities, do not predict the NO_x trap capacities under dynamic conditions. We briefly discuss the steady-state experimental results before describing in detail our experimental results under dynamic conditions.

Steady-State NO_x Adsorption Capacities: Mahzoul et al. (1999) have carried out detailed adsorption experiments on a series of NO_x trap catalysts as a part of their work on the experimental and mechanistic study of NO_x adsorption. The experiments clearly show that the maximum capacity of barium oxide based materials occurs at a temperature of 350–400°C. Furthermore, barium oxide is superior trap than γ-alumina. We have carried out similar experiments on our samples under steady-state conditions and the results are summarized in Table 2. Since alumina also adsorbs a significant fraction of NO_x, the number of barium sites cannot be accurately calculated.

The utilization of all of the available capacity under the dynamic conditions of NO_x trap test with simulated exhaust does not occur. We calculated total amount of NO_x adsorbed per gram of catalyst during the lean cycle. From these data, a fractional coverage achieved during the lean cycle can be estimated by dividing it with the steady-state capacity data (Table 4). The fractional coverage data show that Pt/HBA3 attains the highest capacity utilization ($\sim$ 20%) under dynamic conditions. In our opinion, the estimated fractional coverage data do not offer useful information because there is an implied assumption that saturation coverage under dynamic experimental conditions and steady state conditions are identical.

Trapping Efficiency under Dynamic Conditions: All samples were tested employing a simulated lean burn exhaust gas mixture using an alternating one-minute lean and one-minute rich cycle at 220, 310, 380, 450, and 600°C. The optimum trapping efficiencies for all samples are observed between 310°C and 380°C. Above this temperature, the NO_x trapping efficiencies drop rapidly and are 10% at 600°C. This is in accordance with the thermal decomposition of NO_2 to NO with increasing temperature.

The trapping efficiency test results for Pt/HBA1, Pt/HBA2, Pt/HBA3 are summarized in Figure 7. The maximum trapping efficiencies of Pt/HBA1 and Pt/HBA2 samples, calcined at 600°C, are 25 and 48%, respectively, at 450°C. The trapping efficiencies decrease to 20 and 42% if the samples are calcined 900°C. This decrease in trapping efficien-

Table 4. NO_x Fractional Coverage of Materials During Alternating One Minute Lean-Rich Cycle

Materials	NO_x Adsorption 10^{-6} mol/g·min	Fractional Coverage (%)
Pt/HBA1	9.83	2.02
Pt/HBA2	23.3	5.74
Pt/HBACe	35.8	11.47
Pt/HBA3	42.6	20.3
Pt/MSHBA	51.1	11.18

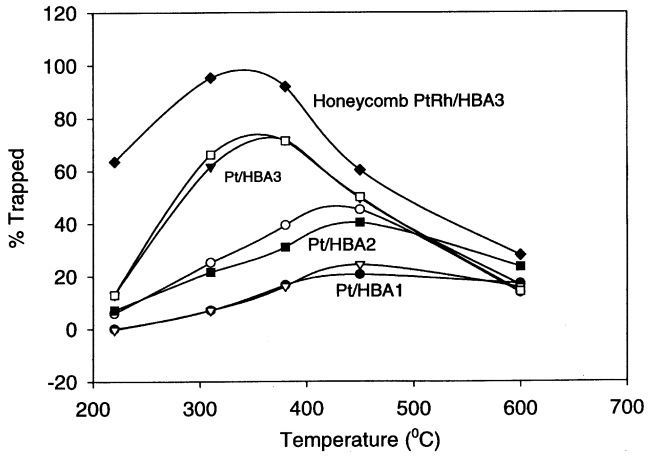

Figure 7. Lean burn NO_x trapping efficiency temperature profile for Pt/HBA1, Pt/HBA2, Pt/HBA3 and Honeycomb PtRh/HBA3 traps fired at 600°C [Hollow] and 900°C [Solid] for 4 h.

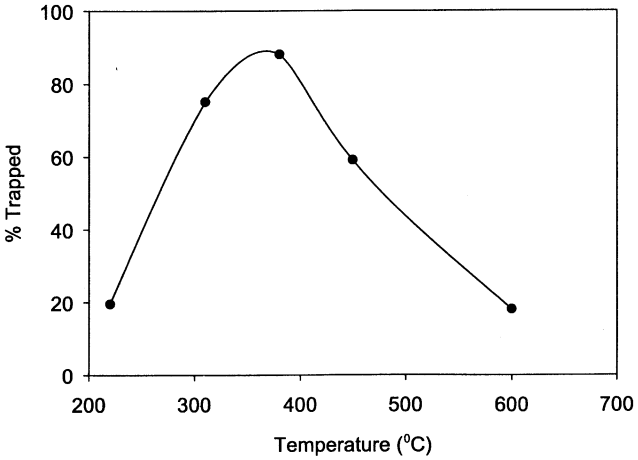

Figure 8. Lean burn NO_x trapping efficiency temperature profile for template assisted sol gel processed $Pt/BaO \cdot 6Al_2O_3$.

cies is due to the decrease in surface area and crystallization of barium aluminate upon calcining at 900°C. Pt/HBA3 exhibits a NO_x trapping efficiency of 70% at 380°C regardless of calcining temperature. This retention of trapping efficiency is due to the stability of HBA3 at elevated temperature. These results show that the NO_x trapping efficiency increases with the decrease in barium oxide content. This can be correlated to the changes in surface properties and material structures with increase in barium oxide content. The highest surface area is observed for the sample with barium oxide close to 20%. This material does not crystallize to barium hexaaluminate structure even after sintering at 900°C. Increase in barium oxide content leads to lower surface area and lower temperature of crystallization to the barium dialuminate structure. Thus, mostly amorphous Pt/HBA3 powders exhibit the highest trapping efficiency of 70% at 380°C among the powder samples.

Freshly prepared Pt/IBA3 also exhibits a 70% NO_x trapping efficiency that is comparable to the Pt/HBA3 samples. It is important to point out that there is a significant difference in Pt/HBA3 and Pt/IBA3. The impregnation generally leads to small barium oxide regions. As a result, a significant portion of impregnated platinum would not be in contact with barium oxide. The amorphous Pt/HBA3, on the other hand, does not exhibit separation of barium oxide or barium aluminate regions. In this material, a large portion of platinum can be expected to be in contact with barium oxide.

The platinum impregnated mesoporous molecular sieves, PT/MSHBA3, exhibit a NO_x trapping efficiency of 86% (Figure 8). The improvement in NO_x trapping efficiency can be assigned to a worm-like pore motif that provides better contact between catalyst and gas molecules.

The Pt/HBACe material exhibits an optimum NO_x trapping efficiency of 60% at 380°C. Interestingly, PtRh/HBACe materials show no improvement in trapping efficiency in comparison with Pt/HBACe materials suggesting that the addition of Rh has no effect on the trapping efficiency of this system (Figure 9).

Among these materials, sol-gel processed HBA3 powder, impregnated with precious metals, offers the optimum combination of thermal stability and NO_x trapping efficiency. We deposited this powder on a honeycomb substrate, impregnated it with 2% Pt and 0.4% Rh, and evaluated it at a 25,000 h^{-1} space velocity. The NO_x trapping efficiency of this catalyst is 95% (cf. 75% for the powder) at 380°C (Figure 7).

Reactions during lean and rich cycles

The changes in the concentration of NO, NO_2 and CO during one lean-rich cycle in the presence of HBA3, Pt/HBA3 and Pt/SG are shown in Figures 10 and 11, respectively. The reactor environment does not instantaneously change from lean to rich and rich to lean with the switchover from O_2 to CO/H_2 pulse and back to O_2 pulse. Complexity of simulated exhaust mixture prevents any useful analysis of data for quantitative information at every step of the rapid switch-over between lean (R range: 1.0–22.22) and rich cycles (R range: 9.13×10^{-3}). Quantitative information can be obtained at the

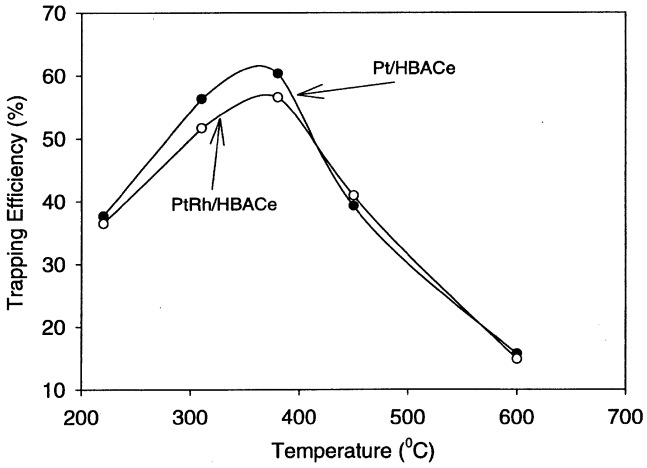

Figure 9. Lean burn NO_x trapping efficiency temperature profiles for Pt/HBACe and Pt/HBACeRh.

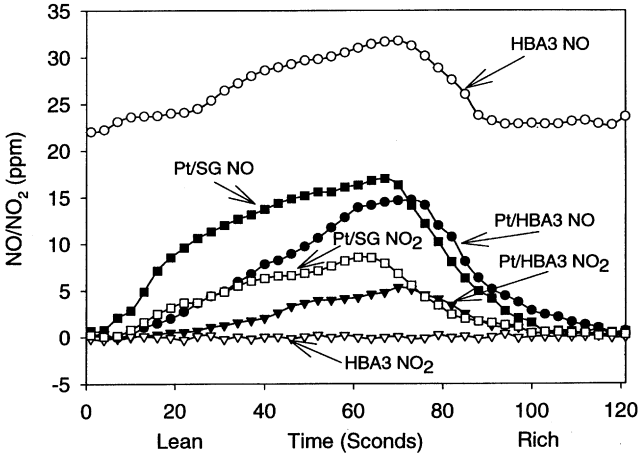

Figure 10. No_x, NO and NO_2 concentrations in one lean-rich cycle employing HBA3, Pt/HBA3 and Pt/SG.

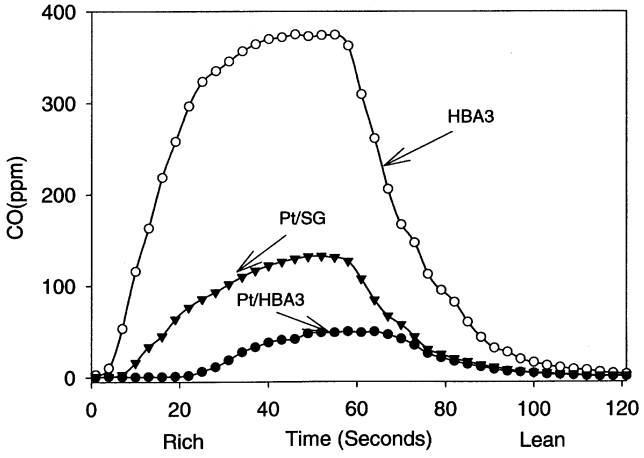

Figure 11. CO concentrations in one lean-rich cycle employing HBA3, Pt/HBA3 and Pt/SG.

midpoints of lean- and rich cycles, however, one should not extrapolate this information to switch-over between cycles. Since the optimum NO_x trapping occurs in 320–380°C range, we limit our discussion to the reactions at 380°C.

Among our samples, HBA3 is ineffective in NO_x oxidation or trapping. At midpoint of the lean cycle of an alternating one-minute lean and rich mode (Figure 10) the Pt/HBA3 catalyst system traps 12 ppm NO_2 and converts 32 ppm NO_x input into 15 ppm NO, 5 ppm NO_2. The presence of 5 ppm NO_2 in gases downstream of the trap suggests that the trap system is unable to convert NO_2 to nitrate and trap it due to the saturation of trapping sites in the vicinity of Pt sites. This is supported by the experiments with Pt/SG sample containing no barium oxide. This sample converts 32 ppm NO_x input into 17 ppm NO, 8 ppm NO_2, and traps 7 ppm NO_2 (Figure 10). Since alumina is not an efficient trapping agent, the amount of NO_2 downstream of Pt/SG trap is larger than that in Pt/HBA3 system. The trapped species in alumina was identified to be a nitrate since the infrared spectrum of this powder showed a 1,386 cm^{-1} peak characteristic of nitrates (Kobayashi et al., 1997).

At the midpoint of the rich cycles, the post HBA3 concentration of NO and CO remains unchanged demonstrating the need for a noble metal catalyst. The post Pt/HBA3 concentration of NO_x decreases to 0 ppm, while 50 ppm CO (Figure 10, Figure 11) and 14 ppm NH_3 are observed (Eq. 4). Since the concentration of ammonia is not sufficient to account for the reduction of NO_x, CO or H_2 assisted reduction must occur.

The NO_x reduction for both Pt/SG and Pt/HBA3 catalysts is almost quantitative. As expected, a large amount of CO is consumed by the Pt/HBA3 system in order to reduce the trapped nitrates (Figure 11). The hydrocarbons do not appear to play an important role because partially oxidized hydrocarbons are not observed in post catalyst gases.

Effect of lean cycle length

In our tests on powders, we found that a one-minute lean cycle is the optimum time for Pt/HBA3 based NO_x traps at 25,000 h^{-1} space velocity and 380°C. If a long lean and short rich cycle is employed, the NO_x trapping efficiencies of Pt/HBA3 and Pt/HBACe are significantly reduced. The trapping efficiency profile of these traps in five-minute lean and one-minute rich cycles are shown in Figure 12. The trapping efficiencies of Pt/HBA3 drop rapidly between first and second minute (15%) reaching to a minimum (7%) between second and third minute. The adsorption also decreases from 47.1×10^{-6} mol/g·min in the first minute to 12.3×10^{-6} and 6.7×10^{-6} mol/g·min in the second and third minutes, respectively. Since the traps have not attained saturation coverage, this rapid decrease can be explained by assuming that the platinum loses its NO_x oxidation ability after first minute because the saturation of adsorbent sites adjacent to platinum limits the removal of NO_2 from platinum sites. The loss in the Pt/HBACe trapping efficiencies is relatively gradual. The adsorption also gradually decreases from 47.2×10^{-6} mol/g·min in the first minute to 29.1×10^{-6} and 23.0×10^{-6} mol/g·min in the second and third minute, respectively. This suggests that cerium oxide slows down the poisoning of platinum. However, it is important to note that the trapping efficiencies of both catalysts after one minute have decreased to an inefficient level.

These results suggest that these NO_x traps cannot be effectively used in a prolonged lean and a short rich cycle at a space velocity of 25,000 h^{-1} at 380°C.

SO_2 poisoning and regeneration

The sulfur-poisoning test was carried out by adding 9 ppm of SO_2 to the test gas mixture. At this dilution, it was not possible to detect SO_2 in outlet gases. Thus, it is not possible to calculate the amount of SO_2 adsorbed in lean cycles. A complete adsorption of SO_2 cannot be assumed because that would suggest a rate of adsorption of 16.8×10^{-6} mol/g·min leading to saturation coverage in 30 min. This would lead to zero percent NO_x trap efficiency after 30 min. Instead, we monitored NO_x trapping efficiency decreases as an indicator of sulfur-poisoning (Figure 13).

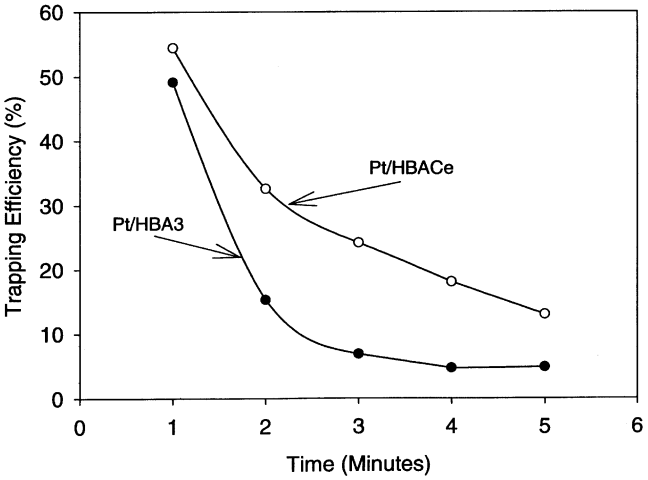

Figure 12. NO_x trapping efficiency vs. time for Pt/HBA3 and Pt/HBACe.

Our experiments show that the NO_x trapping efficiency starts to decrease gradually and 90% of the trapping efficiency of Pt/HBA3 is lost within 24 h. Pt/HBACe loses only 60% of its trapping efficiency.

This decrease in NO_x trapping efficiency occurs because SO_2 oxidizes to SO_3 and competes with NO_2 for trapping sites in $BaO \cdot 6Al_2O_3$ to form sulfates. Furthermore, the gradual saturation of adsorbent sites adjacent to platinum with sulfate reduces the NO_x conversion ability of platinum. The relatively slower poisoning of Pt/HBACe can be attributed to the presence of cerium oxide in the catalyst.

It is important to remember that the oxidation of SO_2 is not limited by catalyst because NO can also oxidize it to SO_3 (King, 1994). Since sulfates do not decompose at 380°C in the rich cycle, the trapping sites become unavailable. All the test materials can be regenerated at 600°C under rich conditions for 40 min (time not optimized). After regeneration, they recover over 90% of their original NO_x trapping efficiency.

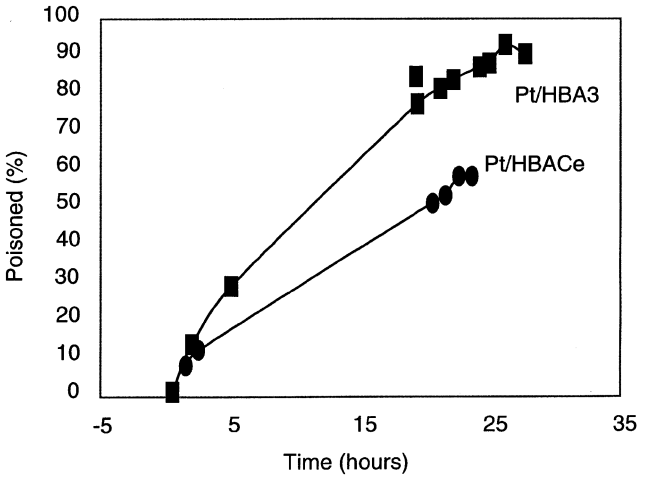

Figure 13. Sulfur poisoning of Pt/HBA3 and Pt/HBACe at 9 ppm SO_2 as a function of time.

Conclusions

There are two important conclusions that can be drawn from this study. First, among $BaO \cdot nAl_2O_3$, $n = 1,2,6$, materials derived from alkoxides by a sol-gel process, $BaO \cdot 6Al_2O_3$ retains its high surface area even after sintering at 900°C. Among $BaO \cdot nAl_2O_3$ materials, the precious metal impregnated $BaO \cdot 6Al_2O_3$ is the best material for NO_x trapping during the lean operation of engines.

The second conclusion relates to the length of lean cycles in alternating lean-rich operation. Our data show that the optimum length of the lean cycle is one minute at 25,000 h^{-1} space velocity. Further increase in the duration of the lean cycle results in the loss of NO_x trapping efficiency. This drop in trapping efficiency can be attributed to the traps' inability to convert NO_2 to NO_3^- (cation Ba^{2+} or Al^{3+}) and trap it.

Acknowledgments

The authors thank Drs. H. S. Gandhi, J. Hepburn, J. Hoard, M. Dearth, and W. Schneider for helpful discussion. We also thank W. Watkins for help in setting up test protocols and catalyst wash coating.

Literature Cited

Adams, K. A., J. V. Cavatio, and R. H. Hameerle, "Lean NO_x Catalysts for Diesel Passenger Cars: Investigating Effects of Sulfur Dioxide and Space Velocity," *Appl. Catal., B*, **10**, 157 (1996).

Bagshaw, S. A., E. Prouzet, and T. J. Pinnavaia, "Templating of Mesoporous Molecular Sieves by Nonionic Polyethylene oxide Surfactants," *Science*, **269**, 1242 (1995).

Bagshaw, S. A., and T. J. Pinnavaia, "Mesoporous Alumina Molecular Sieves," *Angew. Chem., Int. Ed. Engl.*, **35**, 1102 (1996).

Gandhi, H. S., A. G. Piken, M. Shelef, and R. G. Delosh, "Laboratory Evaluation of Three-Way Catalysts," *R. G. SAE Trans.*, **85**, 760201 (1976).

Gierczak, C. A., J. M. Andino, J. W. Butler, G. A. Hesier, G. Jesion, and T. J. Korniski, "FTIR: Fundamentals and Applications in the Analysis of Dilute Vehicle Exhaust," *Measurements of Atmospheric Gases*, SPIE, Vol. 1433, 315 (1991).

Katoh, K., T. Kihara, T. Asanuma, M. Totoh, and N. Shibagaki, "Development of NO_x Storage-Reduction 3-Way Catalyst System for Lean-burn Engines," *Toyota Tech. Rev.*, **44**(2), 30 (1994).

Hepburn, J. S., E. Thanasliu, D. A. Dobson, and W. L. Watkins, "Experimental and Modeling Investigations of NO_x Trap Performance," SAE-962051 (1996).

Hoard, J., and M. L. Balmer, "Analysis of Plasma-Catalysis for Diesel NO_x Remediation," SAE-982429 (1998).

King, R., *Encyclopedia of Inorganic Chemistry*, Wiley, New York (1994).

Kobayashi, T., T. Yamada, and K. Kayano, "Study of NOx Trap Reaction by Thermodynamic Calculation," *Soc. Automot. Eng.*, [Spec. Publ.: Issues in Emissions Control Technology] SP-1248, 63 (1997).

Leenaars, A. F. M., K. Keizer, and A. J. Burggraaf, "The Preparation and Characterization of Alumina Membranes with Ultra-fine Pores. Part 1. Microstructural Investigations on Non-Supported Membranes," *J. Mat. Sci.*, **19**, 1077 (1984).

Machida, M., K. Eguchi, and H. Arai, "Analytical Electron Microscope Analysis of the Formation of $BaO \cdot 6Al_2O_3$," *J. Amer. Ceram. Soc.*, **71**, 1142 (1988).

Mahzoul, H., J. F. Brilhac, and P. Gilot, "Experimental and Mechanistic Study of NOx Adsorption over NOx Trap Catalyst," *Appl. Catal., B*, **20**, 47 (1999).

Mehrotra, R. C., S. Goel, A. B. Goel, R. B. King, and K. C. Nainan, "Preparation and Characterization of Some Volatile Double Isopropoxides of Aluminum with Alkaline Earth Metals," *Inorg. Chim. Acta*, **29**, 131 (1978).

Narula, C. K., "Single-Phase Metal-Alumina Material and its Prepa-

ration by a Sol-Gel Process," U.S. Patent No. 5,403,807 (Apr. 4, 1995).
Narula, C. K., J. E. Allison, D. R. Bauer, and H. S. Gandhi, "Materials Chemistry Issues Related to Advanced Materials Applications in the Automotive Industry," *Chem. Mater.*, **8**, 984 (1996).
Narula, C. K., "Sol-gel Processed Materials in Automotive Exhaust Reduction Catalyst," *Ceramic Trans.*, **73**, 15 (1997).
Narula, C. K., "Sol-Gel Processed Materials in the Automotive Industry," ACS *Symp. Ser.*, **727**, 144 (1999).
Narula, C. K., M. Rokosz, R. Kudla, M. Chattha, and L. F. Allard, "Sol-gel Processed Silica-Alumina Materials for Diesel Engine Emission Reduction Catalysts," *Langmuir*, **16**, 3818 (2000).
Wenzhong, Z., and T. J. Pinnavaia, "Rare Earth Stabilization of Mesoporous Alumina Molecular Sieves Assembled through an N^oI^o Pathway," *Chem. Comm.*, 1185 (1998).

Manuscript received Mar. 6, 2000, and revision received Aug. 11, 2000.